Materials Chemistry and Physics 163 (2015) 402–406

Contents lists available at ScienceDirect

Materials Chemistry and Physics

journal homepage: www.elsevier.com/locate/matchemphys

X-ray diffraction and Mossbauer studies on superparamagnetic nickel ferrite ($NiFe_2O_4$) obtained by the proteic sol–gel method

N.A.S. Nogueira [a, 1], V.H.S. Utuni [b], Y.C. Silva [b], P.K. Kiyohara [c], I.F. Vasconcelos [a], M.A.R. Miranda [b, *], J.M. Sasaki [b]

[a] Departamento de Engenharia Metalúrgica e de Materiais, Centro de Tecnologia, Campus do Pici, Universidade Federal do Ceará – UFC, 60455-760 Fortaleza, CE, Brazil
[b] Departamento de Física, Universidade Federal do Ceará – UFC, Campus do Pici, 60440-970 Fortaleza, CE, Brazil
[c] Instituto de Física, Universidade de São Paulo – USP, 05315-970 São Paulo, SP, Brazil

HIGHLIGHTS

- Superparamagnetic nickel ferrite nanoparticles were grown by the proteic sol–gel method.
- The proteic sol–gel method provided superparamagnetic nickel ferrite nanoparticles with sizes in the range of 9–13 nm.
- Nickel ferrite nanoparticles were prepared at temperatures as low as 250 °C.
- The nickel ferrite nanoparticles were studied by x-ray diffraction and Mossbauer.

ARTICLE INFO

Article history:
Received 26 November 2014
Received in revised form
5 July 2015
Accepted 21 July 2015
Available online 1 August 2015

Keywords:
Nanostructures
Magnetic materials
Powder diffraction
Mossbauer effect
Sol–gel growth
Microstructure

ABSTRACT

Nickel ferrite ($NiFe_2O_4$) nanoparticles were synthesized by the proteic sol–gel method at synthesis temperature of 250 °C, 300 °C and 400 °C, with the objective of obtaining superparamagnetic nanoparticles. Thermogravimetric analysis (TGA) and temperature-programed oxidation (TPO) presented peaks around 290 °C indicating that nickel ferrite was forming at this temperature. X-ray powder diffraction (XRPD) confirmed that the polycrystalline sample was single phased $NiFe_2O_4$ with space group Fd3m. Scherrer equation applied to the diffraction patterns and transmission electron microscopy (TEM) images showed that the size of the nanoparticles ranged from 9 nm to 13 nm. TEM images also revealed that the nanoparticles were agglomerated, which was supported by the low values of surface area provided by the Brunauer-Emmet-Teller (BET) method. Mossbauer spectroscopy presented spectra composed of a superposition of three components: a sextet, a doublet and a broad singlet pattern. The sample synthetized at 300 °C had the most pronounced doublet pattern characteristic of superparamagnetic nanoparticles. In conclusion, this method was partially successful in obtaining superparamagnetic nickel ferrite nanoparticles, in which the synthetized samples were a mixture of nanoparticles with blocking temperature above and below room temperature. Magnetization curves revealed a small hysteresis, supporting the Mossbauer results. The sample with the higher concentration of superparamagnetic nanoparticles being the one synthetized at 300 °C.

© 2015 Elsevier B.V. All rights reserved.

1. Introduction

Ferrites are a large class of oxides with an interesting set of properties: high saturation magnetization and electrical resistivity, low dielectric losses and a good physical and chemical stability [1]. These properties allow a wide range of applications such as in magnetic resonance imaging contrast agents for biotechnology [1,2], gas sensors [3,4], microwave devices [5], carries for targeted drug delivery [6,7] and magnetic nanofluid for hyperthermia cancer treatments [8–10]. There are several routes for preparations of ferrites that include: mechanochemical [11], sol–gel processing [12–14], co-precipitation [15,16], combustion [17,18], hydrothermal

* Corresponding author.
E-mail address: marcus.a.r.miranda@gmail.com (M.A.R. Miranda).
[1] Present address: Departamento de Ciências Exatas, Tecnológicas e Humanas, Campus Angicos, Universidade Federal Rural do Semi-árido – UFERSA, 59.515-000 Angicos, RN, Brazil.

http://dx.doi.org/10.1016/j.matchemphys.2015.07.057
0254-0584/© 2015 Elsevier B.V. All rights reserved.

[19], reverse micelle [20] and other methods.

In this work, nickel ferrite ($NiFe_2O_4$) was synthesized by the proteic sol–gel method. In this method, gelatin has been used as the polymeric agent due to its solubility in water and ability to bond with metal ions in solution, which simplifies the process and reduces the cost of synthesis when compared to conventional sol–gel methods. Several metal oxides and alloys were already obtained through this method [21–24].

The thermal decomposition behavior of the $NiFe_2O_4$ powder was examined by means of thermogravimetry (TG) and differential thermal analysis (DTA). The morphology and structure were examined by Brunauer-Emmet-Teller (BET), X-ray powder diffraction (XRPD) and Transmission Electron Microscopy (TEM). Average particle sizes were calculated by the Scherrer's equation [25] using the results of the Rietveld refinement [26]. The superparamagnetic behavior was investigated with Mossbauer spectroscopy.

2. Experimental procedures

The proteic solution was prepared dissolving nickel nitrate hexahydrate – $Ni(NO_3)_3.6H_2O$ (Sigma–Aldrich 97%) and iron nitrate nonahydrate – $Fe(NO_3)_3.9H_2O$ (Sigma–Aldrich 98%) in gelatin solution (Gelita™) prepared with distilled water. The molar ratio of the nickel nitrate to iron nitrate was 1:2 and the sum of the masses of the nitrates was twice the mass of gelatin. The gel formed by the mixture of the nickel nitrate, iron nitrate and gelatin was then dried at 100 °C for 24 h resulting in a spongy and voluminous product.

After drying, the mixture was macerated, resulting in a fine powder. A portion of this powder was used for the thermal analysis TG and DTA, while the remaining part was divided in three portions and calcined for 4 h in a rotating furnace at different temperatures (250 °C, 300 °C and 400 °C with a heating rate of 10 °C/min). After calcination, the powder was mixed on a Becker with hydrogen peroxide (5 mL) for 10 min, aimed at dissolving the remaining organic matter in the sample. Finally, the samples were washed two times in centrifuge tubes (Quimis, model Q222T) with distilled water and dried in the oven at 100 °C for 24 h.

In order to monitor the mass change of the samples during heating, TG and DTA experiments were conducted under synthetic air with a heating rate of 10 °C/min, on a Netzsch STA 409 PC/PG. Temperature programmed oxidation (TPO) experiments were carried in the powder (9.4 mg), with a heating rate of 10 °C/min, under air atmospheric conditions.

The structural characterization of all samples was carried out by XRPD at room temperature using a Panalytical X'Pert PRO - model MPD diffractometer, with a hybrid monochromator and cobalt characteristic radiation ($\lambda = 1.78896$ Å), at 40 kV × 30 mA. The diffraction patterns were indexed using the International Centre for Diffraction Data (ICDD). The structural parameters and atomic positions were refined by the Rietveld method, using Gsas [27]/Expgui [28] software. These results were used to calculate average particle size using Scherrer's equation, $D = (k\lambda)/(\beta cos\theta)$, in which $k = 1.0747$, considering spherical particles with cubic symmetry [29], θ is the Bragg angle and β is full-width at half maximum (FWHM) of the diffraction peaks, corrected for instrumental broadening. Specific surface area was estimated by Brunauer–Emmett–Teller (BET) method using Autosorb-1, Quantachrome Instruments, with degassing time of 5 h and helium gas as purging agent, and using N_2 adsorption at 77K. The morphology and particle-size distribution were investigated by TEM, using a Philips CM200 microscope. ^{57}Fe Mossbauer measurements were carried out at room temperature using a ^{57}Co radioactive source in a sinusoidal velocity pattern in transmission mode. Magnetization curves were obtained in a Vibrating Sample Manetometer at room temperature and with a maximum applied field of 12.5 kOe.

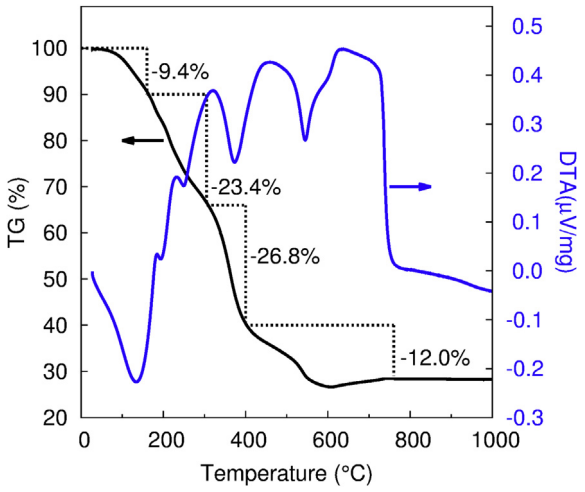

Fig. 1. DTA/TG curves of the dried mixture of nickel nitrate, iron nitrate and gelatin.

3. Results and discussion

The TG - DTA results shown in Fig. 1 help in the selection of the calcination temperature. The mass loss event below 160 °C is associated with dehydration, as indicated by the endothermic peak at 130 °C in the DTA curve, while the weight loss in the temperature

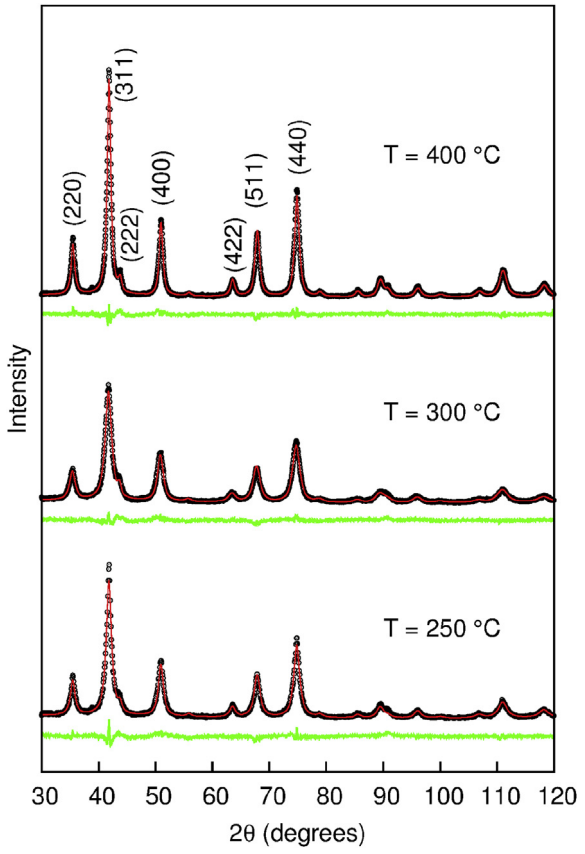

Fig. 2. XRPD patterns of the $NiFe_2O_4$ nanoparticles synthesized by the proteic sol–gel method at different temperatures (black circles) together with the result of the calculated pattern obtained with Rietveld refinement (red line). The green line is the difference between the experimental and calculated intensities. (For interpretation of the references to colour in this figure legend, the reader is referred to the web version of this article.)

Table 1
Rietveld refinement, surface area and Scherrer's equation results for the $NiFe_2O_4$ nanoparticles synthesized by the proteic sol–gel method.

Sample/Temperature (°C)	Particle size[a] (nm)	Lattice parameter (Å)	Rwp (%)	Specific surface area (BET) (m^2/g)
250	10	8.34 ± 0.01	9.56	14.6
300	9	8.33 ± 0.01	9.27	88.6
400	13	8.34 ± 0.01	7.87	13.6

[a] Calculated using Scherrer's equation.

range of 160–290 °C corresponds to the decomposition o gelatin, elimination of organic matter and subsequently release of CO and CO_2 gases. A large exothermic peak in the TPO results at 288 °C confirms the release of these gases. The mass loss between 290 °C and 760 °C is related to further organic decomposition and formation of oxides, for instance the small mass increase near 600 °C in the TG curve may indicate oxygen gain. For temperatures above 760 °C the system stabilizes and the total mass loss is 72% which is very close to the theoretical value of 75% that is calculated considering the masses of the gelatin and the iron and nickel nitrates used.

Considering the combustion event indicated by the TPO at 288 °C and the endothermic peak in the DTA curve at 290 °C, all probably related to the beginning of oxide formation, and knowing that high temperatures lead to large particle size, low temperatures were selected for calcination: 250 °C, 300 °C and 400 °C.

The XRPD patterns for the samples annealed at 250 °C, 300 °C and 400 °C are shown in Fig. 2 and present only the cubic (Fd3m) $NiFe_2O_4$ phase, while the fitting of the sharp diffraction peaks at high-angles indicate good crystallinity [30]. The Rietveld refinement was used to extract the line broadening of the diffraction peaks and input it into the Scherrer's equation, which gave particle sizes ranging from 9 to 13 nm (see Table 1). The fitting quality was checked through the reliability factor Rwp that was within the 10% range suggested in the literature [31].

BET results are shown in Table 1 and present an anomaly for the sample synthesized at 300 °C, for which the surface area value is about 6 times that of the other samples. It is expected that smaller particle sizes lead to larger surface areas and indeed this sample has the smaller particle size. However, the difference in particle sizes presented in Table 1 does not explain the surface area values. Considering a simplified model where the powder is composed of dispersed spheres, the variation in surface area due to particle size alone is a lot less than six fold, which suggests that another mechanism is responsible for these values, possibly agglomeration and porosity. It is relevant to notice that at 300 °C there is a significant exothermic transformation as shown in the DTA (see Fig. 1) and TPO results and that the minima of this transformation are very close to 250 °C and 400 °C. It is reasonable to suppose that this transformation is responsible for the dispersion in the nanocrystalline particles leading to a surge in the surface area when compared to the samples synthesized at 250 °C and 400 °C. Further investigation is necessary.

The TEM images of $NiFe_2O_4$ at temperatures 250 °C, 300 °C and 400 °C are shown in Fig. 3. The tendency of agglomeration was observed in all samples; this is expected for particles with these sizes, in which the surface energy is high because of the large surface to volume ratio. Therefore, there is a large number of atoms with incomplete coordination. These particles then try to stabilize themselves by lowering their surface energy forming bonds with adjacent particles, these bonds being covalent, ionic, metallic or vander Walls depending on the material. The distribution of particle sizes was measured by imaging software (image J) [32]; the results of this analysis are presented in Fig. 4. The crystalline grains are randomly oriented in each sample. The average particle sizes estimated from TEM were 9.2 nm, 7.9 nm and 15.4 nm for 250 °C, 300 °C and 400 °C, respectively. This result was consistent with the results of Scherrer's equation. The sample of 300 °C presents higher concentrations of smaller particles (Fig. 4), but then again it does not explain the value of the surface area (88.6 m^2/g), well above the values of the samples of 250 °C and 400 °C.

Fig. 5 shows the Mossbauer spectra taken at room temperature of the nanoparticles synthesized at 250 °C, 300 °C and 400 °C and Table 2 shows the hyperfine parameters. The values of the hyperfine parameters were obtained by least square fitting of lorentzian distribution functions. These spectra are typically a superposition of three components: a sextet, a doublet and a broad singlet pattern.

Fe atoms occupy ferromagnetic sites in the nickel ferrite spinel structure. These sites present themselves in the Mossbauer spectra

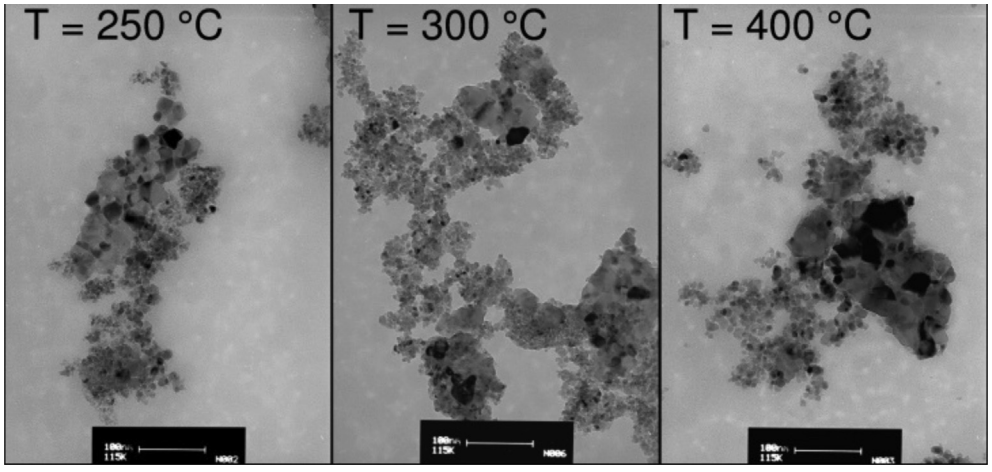

Fig. 3. Transmission electron micrographs of the $NiFe_2O_4$ nanoparticle powder for samples synthesized at 250 °C, 300 °C and 400 °C. The scale in the figure is 100 nm.

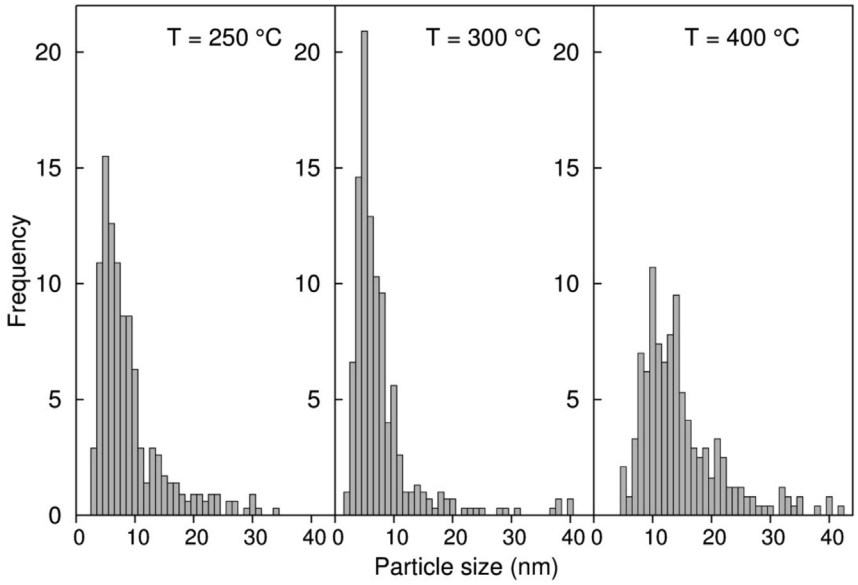

Fig. 4. Particle size histograms obtained from the transmission electron micrographs of the $NiFe_2O_4$ nanoparticle powder for samples synthesized at 250 °C, 300 °C and 400 °C.

as two sextets as shown in the spectra for T = 1000 °C in Fig. 5 [14]. It is known that the blocking temperature of the ferromagnetic interactions is proportional to the particle size and that for $NiFe_2O_4$ nanoparticles this temperature is around room temperature. Then, the reduction of particle size, and consequently the reduction of the ferromagnetic blocking temperature, implies in the weakening of the ferromagnetic interactions causing a broadening in the sextet lines and also a reduction in the hyperfine magnetic field. Further reduction of the particle size, leading to the limit of blocking the ferromagnetic interactions, causes a collapse in the sextet therefore forming a broad lined singlet. Particles with size below the blocking limit give rise to a superparamagnetic doublet. There features can be seen in the spectra of the nanoparticles synthetized at 250 °C, 300 °C and 400 °C, in which TEM results show a large distribution in particle size indicating that the sample present nanoparticles with blocking temperature above and below room temperature [14].

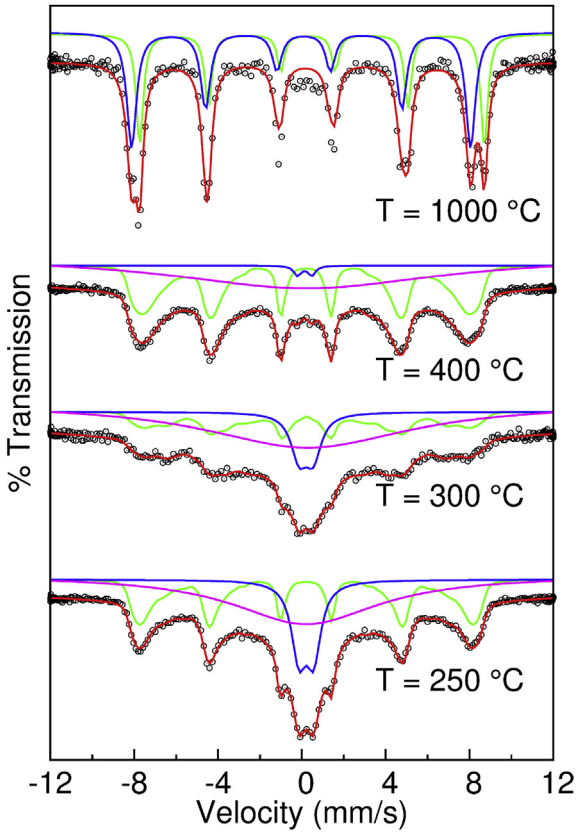

Fig. 5. Room temperature ^{57}Fe Mossbauer spectra of the $NiFe_2O_4$ nanoparticles synthesized by the proteic sol–gel method at different temperatures.

The magnetic measurements were performed at room temperature; Table 3 contains the magnetic properties of the nickel ferrite nanoparticles and Fig. 6 shows the magnetization curve for the sample prepared at 300 °C. From the magnetization curves one can observe that there was a reduction in the maximum magnetization and an increase in the coercive field (H_c) for the sample prepared at 300 °C probably due to the surface effect that contributed to an increased cationic disorder [30,33]. In this sample a decrease in the coercive field was expected, however this property is influenced by nanoparticle size, anisotropy and lattice strain [34]; The TEM images (Fig. 3) display the tendency of the $NiFe_2O_4$ nanoparticle to agglomerate and the histograms (Fig. 4) present a considerable size distribution for these nanoparticles. The high concentration of

Table 2
Hyperfine parameters obtained from fitting Mossbauer spectra.

Sample	Site	δ (mm/s)	Δ (mm/s)	Bhf (T)	Γ (mm/s)	Area (%)
250 °C	Sextet	0.31	0.00	48	0.30	27.5
	Doublet	0.32	0.69		0.84	16.5
	Singlet	0.31			8.46	56.0
300 °C	Sextet	0.34	0.00	41	0.30	20.0
	Doublet	0.31	0.67		0.92	10.0
	Singlet	0.39			11.94	70.0
400 °C	Sextet	0.30	0.00	47	0.30	33.5
	Doublet	0.24	0.67		0.41	1.0
	Singlet	0.33			15.71	65.5
1000 °C	Sextet (B)	0.36	0.00	52	0.40	61.0
	Sextet (A)	0.26	0.00	49	0.47	39.0

δ – isomer shift; Δ – quadrupole splitting; Bhf – hyperfine magnetic field; Γ - width of the spectral line; A – tetrahedral site; B – octahedral site.

Table 3
Magnetic properties obtained from VSM.

Sample	M_{max} (emu/g)	M_r (emu/g)	H_c (Oe)
250 °C	28.7	1.9	70
300 °C	26.8	4.0	210
400 °C	28.0	1.7	60

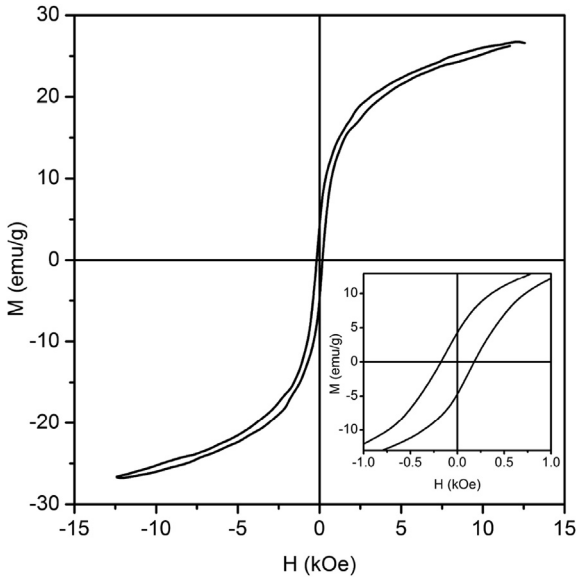

Fig. 6. Magnetization curve of nickel ferrite nanoparticle prepared at 300 °C.

nanoparticles with sizes smaller than the blocking limit, as supported by the BET and Mossbauer spectroscopy, favors the superparamagnetic behavior of this sample, however, because of the large size distribution, this behavior could not be observed in the magnetization curves.

4. Conclusions

The proteic sol–gel method was effective for obtaining nanoparticles of $NiFe_2O_4$ at low temperatures of synthesis (250 °C–400 °C) with sizes in the range of 9–13 nm, confirmed by X-ray powder diffraction and transmission electron microscopy. Mossbauer spectroscopy showed evidence that samples were in part, composed of superparamagnetic nanoparticles, and the sample synthesized at 300 °C contained the largest fraction of superparamagnetic nanoparticles.

Acknowledgment

The authors would like to thank financial support from the Brazilian agency CNPq – Brazil, process number 140078/2009-6. We also thank Dr. V. N. Freire (UFC) for BET analysis.

References

[1] R. Valenzuela, Novel applications of ferrites, Phys. Res. Int. (2012) 1–9.
[2] H.B. Na, I.C. Song, T. Hyeon, Inorganic nanoparticles for MRI contrast agents, Adv. Mater 21 (2009) 2133–2148.
[3] S.L. Darshane, S.S. Suryavanshi, I.S. Mulla, Nanostructured nickel ferrite: a liquid petroleum gas sensor, Ceram. Int. 35 (2009) 1793–1797.
[4] A.B. Gadkari, T.J. Shinde, P.N. Vasambekar, Ferrite Gas sensors, IEEE Sens. J. 11 (2011) 849–861.
[5] A. Hannour, D. Vincent, F. Kahlouche, A. Tchangoulian, S. Neveu, V. Dupuis, Self-biased cobalt ferrite nanocomposites for microwave applications, J. Magn. Magn. Mater 353 (2014) 29–33.
[6] M. Mahmoudi, S. Sant, B. Wang, S. Laurent, T. Sen, Superparamagnetic iron oxide nanoparticles (SPIONs): development, surface modification and applications in chemotherapy, Adv. Drug Deliv. Rev. 63 (2010) 24–46.
[7] S. Rana, A. Gallo, R.S. Srivastava, R.D.K. Misra, On the suitability of nanocrystalline ferrites as a magnetic carrier for drug delivery: functionalization, conjugation and drug release kinetics, Acta Biomater. 3 (2007) 233–242.
[8] I. Sharifi, H. Shokrollahi, S. Amiri, Ferrite-based magnetic nanofluids used in hyperthermia applications, J. Magn. Magn. Mater 324 (2012) 903–915.
[9] A.B. Salunkhe, V.M. Khot, S.H. Pawar, Magnetic hyperthermia with magnetic nanoparticles: a status review, Curr. Top. Med. Chem. 14 (2014) 572–594.
[10] O.S. Nielsen, M. Horsman, J. Overgaard, A future for hyperthermia in cancer treatment? Eur. J. Cancer 37 (2001) 1587–1589.
[11] H. Yang, X. Zhang, W. Ao, G. Qiu, Formation of NiFe2O4 nanoparticles by mechanochemical reaction, Mater. Res. Bull. 39 (2004) 833–837.
[12] M. Mozaffari, J. Amighian, E. Darsheshdar, Magnetic and structural studies of nickel-substituted cobalt ferrite nanoparticles, synthesized by the sol–gel method, J. Magn. Magn. Mater 350 (2014) 19–22.
[13] J.G.S. Duque, E.A. Souza, C.T. Meneses, L. Kubota, Magnetic properties of NiFe O nanoparticles produced by a new chemical method, Phys. B 398 (2007) 287–290.
[14] A. Ahlawat, V.G. Sathe, V.R. Reddy, A. Gupta, Mossbauer, raman and X-ray diffraction studies of superparamagnetic NiFe2O4 nanoparticles prepared by sol–gel auto-combustion method, J. Magn. Magn. Mater 323 (2011) 2049–2054.
[15] A.S. Albuquerque, J.D. Ardisson, W. Macedo, J.L. López, R. Paniago, A.I.C. Persiano, Structure and magnetic properties of nanostructured Ni-ferrite, J. Magn. Magn. Mater (2001) 226–230.
[16] S. Neveu, A. Bee, M. Robineau, D. Talbot, Size-selective chemical synthesis of tartrate stabilized cobalt ferrite ionic magnetic fluid, J. Colloid Interface Sci. 255 (2002) 293–298.
[17] M.R. Phadatare, V.M. Khot, A.B. Salunkhe, N.D. Thorat, S.H. Pawar, Studies on polyethylene glycol coating on NiFe2O4 nanoparticles for biomedical applications, J. Magn. Magn. Mater 324 (2012) 770–772.
[18] A.C.F.M. Costa, R.T. Lula, R.H.G.A. Kiminami, L.F.V. Gama, A.A. Jesus, H.M.C. Andrade, Preparation of nanostructured NiFe2O4 catalysts by combustion reaction, J. Mater. Sci. 41 (2006) 4871–4875.
[19] Y. Cheng, Y. Zheng, Y. Wang, F. Bao, Y. Qin, Synthesis and magnetic properties of nickel ferrite nano-octahedra, J. Solid State Chem. 178 (2005) 2394–2397.
[20] A. Kale, S. Gubbala, R.D.K. Misra, Magnetic behavior of nanocrystalline nickel ferrite synthesized by the reverse micelle technique, J. Magn. Magn. Mater 277 (2004) 350–358.
[21] A.M.L. Medeiros, M.A.R. Miranda, A.S. Menezes, P.M. Jardim, L.R.D. Silva, S.T. Gouveia, J.M. Sasaki, Synthesis and characterization of Cr_2O_3 nanoparticles obtained by gelatin, J. Metastable Nanocryst. Mater. 20–21 (2004) 399–404.
[22] A.O.G. Maia, C.T. Meneses, A.S. Menezes, W.H. Flores, D.M.A. Melo, J.M. Sasaki, Synthesis and X-ray structural characterization of NiO nanoparticles obtained through gelatin, J. Non-Cryst. Solids 352 (2006) 3729–3733.
[23] C.T. Meneses, W.H. Flores, J.M. Sasaki, Direct observation of the formation of nanoparticles by in situ time-resolved x-ray absorption spectroscopy, Chem. Mater 19 (2007) 1024–1027.
[24] N.A.S. Nogueira, E.B. da Silva, P.M. Jardim, J.M. Sasaki, Synthesis and characterization of NiAl2O4 nanoparticles obtained through gelatin, Mater. Lett. 61 (2007) 4743–4746.
[25] L.V. Azzarof, M.J. Buerger, The Powder Method in X-ray Crystallography, McGraw-Hill Book Company, 1958.
[26] H.M. Rietveld, Line profiles of neutron powder-diffraction peaks for structure refinement, Acta Crystallogr. 22 (1967) 151–152.
[27] A.C. Larson, R.B. Von Dreele, General Structure Analysis System (GSAS), Los Alamos National Laboratory, LAUR, 2004, 86–748.
[28] B.H. Toby, EXPGUI, a graphical user interface for ıt GSAS, J. Appl. Crystallogr. 34 (2001) 210–213.
[29] R.W. James, The Optical Principles of the Diffraction of X-rays, the Crystalline State, vol. II, G. Bell and Sons Ltd, 1962.
[30] J. Wang, Prepare highly crystalline NiFe2O4 nanoparticles with improved magnetic properties, Mater. Sci. Eng. B 127 (2006) 81–84.
[31] S.M. Patange, S.E. Shirsath, S.S. Jadhav, K.S. Lohar, D.R. Mane, K.M. Jadhav, Rietveld refinement and switching properties of Cr3+ substituted NiFe2O4 ferrites, Mater. Lett. 64 (2010) 722–724.
[32] Rasband W ImageJ - Image Processing and Analysis in Java.
[33] M.H. Mahmoud, A.M. Elshahawy, S.A. Makhlouf, H.H. Hamdeh, Mossbauer and magnetization studies of nickel ferrite nanoparticles synthesized by the microwave-combustion method, J. Magn. Magn. Mater. 343 (2013) 21–26.
[34] K. Nejati, R. Zabihi, Preparation and magnetic properties of nano size nickel ferrites particles using hydrothermal method, Chem. Central J. 23 (2012) 1–6.